

Superconductivity in SrB₃C₃ clathrate

Li Zhu,¹ Hanyu Liu,^{1,2} Maddury Somayazulu,³ Yue Meng,³ Piotr A. Guńka ^{1,4} Thomas B. Shieff,¹ Curtis Kenney-Benson,³ Stella Chariton,⁵ Vitali B. Prakapenka,⁵ Hyeok Yoon,⁶ Jarryd A. Horn,⁶ Johnpierre Paglione,^{6,7} Roald Hoffmann,⁸ R. E. Cohen ¹ and Timothy A. Strobel ¹

¹*Earth and Planets Laboratory, Carnegie Institution for Science, 5241 Broad Branch Road, NW, Washington, DC 20015, USA*

²*International Center for Computational Method and Software and State Key Laboratory of Superhard Materials, College of Physics, Jilin University, Changchun 130012, China*

³*HPCAT, X-ray Science Division, Argonne National Laboratory, Lemont, Illinois 60439, USA*

⁴*Faculty of Chemistry, Warsaw University of Technology, Noakowskiego 3, 00-664 Warszawa, Poland*

⁵*Center for Advanced Radiation Sources, University of Chicago, Chicago, Illinois 60439, USA*

⁶*Maryland Quantum Materials Center, Department of Physics, University of Maryland, College Park, 20742 Maryland, USA*

⁷*The Canadian Institute for Advanced Research, Toronto, Ontario, Canada M5G 1Z8*

⁸*Department of Chemistry and Chemical Biology, Baker Laboratory, Cornell University, Ithaca, New York 14853-1301, USA*



(Received 26 May 2021; revised 16 November 2022; accepted 23 November 2022; published 12 January 2023)

We predict superconductivity for the carbon–boron clathrate SrB₃C₃ with $T_c = 27\text{--}43$ K for Coulomb pseudopotential (μ^*) values between 0.17 and 0.10 using first-principles calculations with conventional electron–phonon coupling. Electrical transport measurements, facilitated by an *in situ* experimental design compatible with extreme synthesis conditions (> 3000 K at 50 GPa), show nonhysteretic resistivity drops that track the calculated magnitude and pressure dependence of superconductivity for $\mu^* \approx 0.15$, and transport measurements collected under applied magnetic fields indicate superconductivity with an onset T_c of approximately 20 K at 40 GPa. Carbon-based clathrates thus represent a class of superconductors similar to other covalent metals like MgB₂ and doped fullerenes. Carbon clathrates share structures similar to superconducting superhydrides with wide potential for tunable properties, and covalent C–B bonds allow metastable persistence at ambient conditions.

DOI: [10.1103/PhysRevResearch.5.013012](https://doi.org/10.1103/PhysRevResearch.5.013012)

I. INTRODUCTION

Since superconductivity was first discovered in elemental mercury [1], the search for superconductors with high transition temperatures (T_c) has represented an active area of research for more than a century. While much progress has been made in the field of unconventional superconductors (i.e., cuprates [2,3] and iron-pnictides [4–6]), the underlying mechanisms for these materials remain controversial, which creates challenges for the design of new higher- T_c materials. On the other hand, recent high-pressure studies on hydride materials [7–20] have pushed superconductivity closer to room temperature. The superconducting mechanisms of these hydrides appear to be well-described by the Eliashberg theory of phonon-mediated superconductivity, and density-functional theory (DFT) predicts their electronic structures, phonons, and electron–phonon coupling quite well [21,22]. In this case, high-frequency phonons account for a large portion of the high superconducting transition temperature; thus,

materials containing light elements have been considered optimal candidates for high- T_c superconductivity [23].

As the lightest element, metallic hydrogen was first considered to be a high-temperature superconductor [24], followed by several high- T_c (super)hydrides based on the concept of chemical precompression [7–20,25]. Current evidence suggests that these materials [7–20,25] are electron–phonon superconductors, and that DFT computations may be used to guide experiments. Indeed, H₃S [8,26–28], LaH₁₀ [11,13,16,29,30], and others [31–36] were predicted to be high- T_c superconductors before experiments were performed. Recent predictions even suggest the possibility for above-room-temperature superconductivity in Li₂MgH₁₆ [12]. Many of the high- T_c superhydrides adopt clathrate-like structures in which H atomic positions represent the vertices of polyhedral cages and weak bonds between H atoms represent cage edges, similar to tetrahedral clathrate host lattices [37–42]. To date, all known superhydride materials decompose at low pressures (most superhydrides are formed above 150 GPa). Stabilization of superhydride superconductors at ambient conditions presents a major challenge, and an open fundamental question is whether other light-element compounds can approach the high- T_c values observed for superhydrides, but at reduced pressures.

Other light-element compounds aside from hydrides also exhibit superconductivity and possess strong covalent bonds that enable their persistence at ambient pressure. For

Published by the American Physical Society under the terms of the [Creative Commons Attribution 4.0 International](https://creativecommons.org/licenses/by/4.0/) license. Further distribution of this work must maintain attribution to the author(s) and the published article's title, journal citation, and DOI.

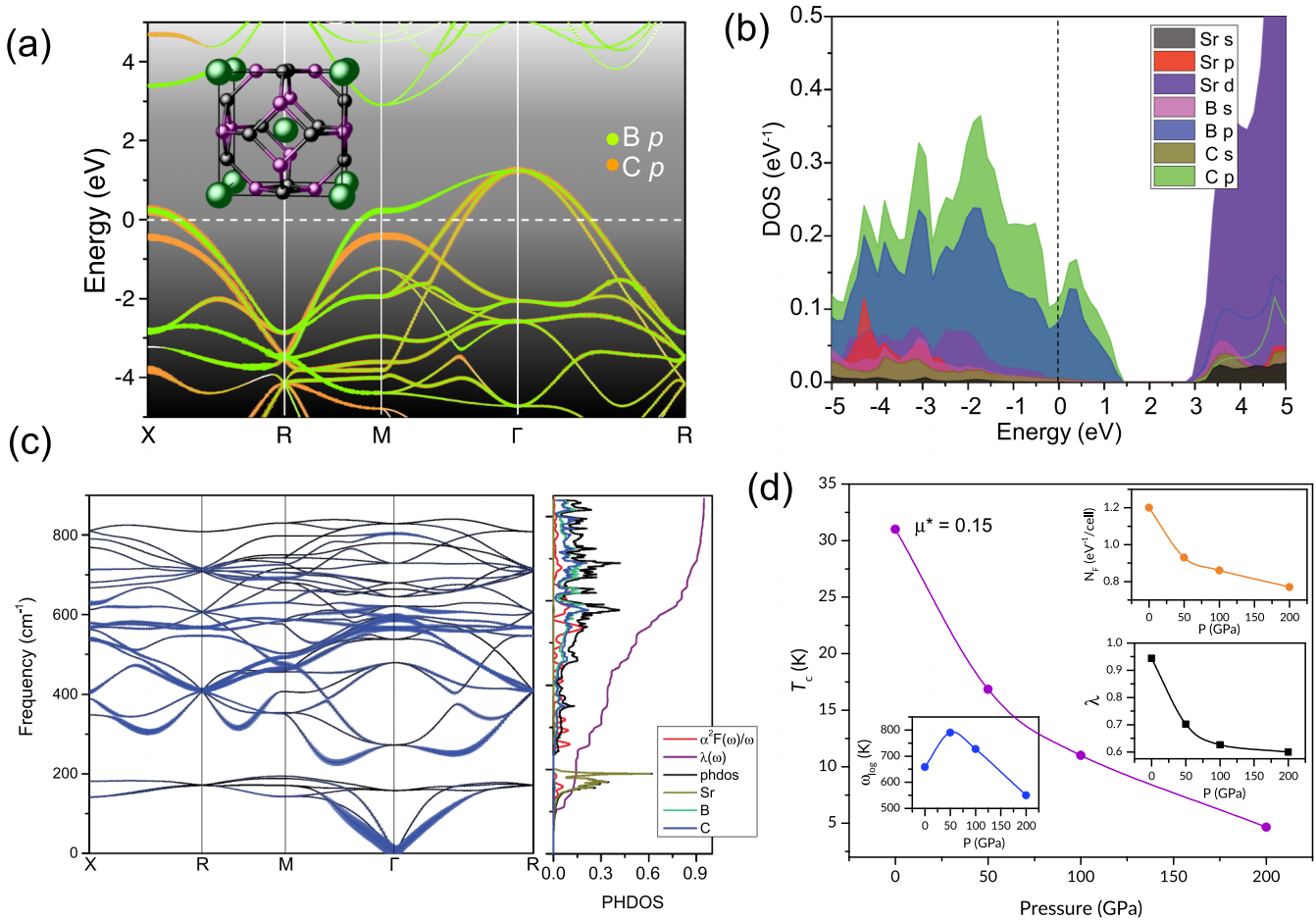


FIG. 1. (a) Electronic band structure for SrB_3C_3 at 0 GPa. The bands projected onto the B p and C p orbitals are displayed with green and orange points, respectively. The size of each point is proportional to the weight of the orbital character. The inset shows the crystal structure of the SrB_3C_3 clathrate with green, purple, and black spheres representing Sr, B, and C atoms, respectively. (b) Projected DOS in SrB_3C_3 . The dashed line indicates the Fermi energy. (c) Phonon dispersion, phonon density of states (PHDOS), phonon spectroscopic function $\alpha^2F(\omega)/\omega$ and electron-phonon integral $\lambda(\omega)$ of SrB_3C_3 at 0 GPa. The size of blue circles in the phonon dispersion curves is proportional to the electron-phonon coupling strength. (d) Calculated T_c as a function of pressure with $\mu^* = 0.15$. The pressure dependencies of ω_{\log} , N_F , and λ are shown as insets.

example, MgB_2 is the highest-temperature conventional superconductor known at atmospheric pressure with $T_c = 39$ K [43]. Structurally similar to MgB_2 , superconductivity ($T_c < 5$ K) was demonstrated for MB_2C_2 ($M = \text{rare-earth metal}$) compounds, and higher T_c 's have been predicted for MB_2C_2 compounds containing alkali and alkaline-earth metals [44–46]. Doped diamond [47–49] and fullerenes [50] also exhibit moderately high T_c . Recently, superconductivity was predicted in undoped diamond via compression-shear deformation [51] and in boron-carbon compounds [52]. Carbon-based clathrates, sharing similar structures to the high-pressure superhydrides, were predicted to exhibit high- T_c superconductivity at atmospheric pressure. For example, $T_c \approx 119$ K was predicted for Na-filled carbon clathrate in the sodalite structure [53], and $T_c \approx 77$ K was predicted for type-II carbon clathrate doped with fluorine guest atoms [54]. In these cases, sp^3 bonding may facilitate large electron-phonon coupling [55]. Nevertheless, carbon clathrate structures represent challenging synthetic targets due to large formation energies.

Using a combination of swarm-intelligence based structure prediction methods [56–58] and high-pressure experi-

ments, we recently predicted and synthesized a carbon-based clathrate, SrB_3C_3 [Fig. 1(a)], which is stabilized by boron substitution into the host framework [59]. SrB_3C_3 is metallic with an appreciable density of states at the Fermi energy, suggesting the potential for superconductivity at moderately high temperature. Here, we predict superconductivity for SrB_3C_3 using first-principles electron-phonon calculations and report experimental electrical transport measurements that are consistent with the calculations. Our results suggest that the SrB_3C_3 clathrate exhibits a moderately high T_c of ~ 22 K at 23 GPa, which is estimated to increase to ~ 31 K at ambient pressure.

II. METHODS

A. Calculations

First-principles calculations were primarily performed in the framework of density-functional theory within the Perdew-Burke-Ernzerhof [60] generalized gradient approximation [61] as implemented in the VASP (Vienna *Ab initio* Simulation Package) code [62]. We also adopted the SCAN

functional [63] that yields accurate electronic structures [64], and agrees with PBE results. The projector-augmented wave (PAW) method [65] was adopted with the PAW potentials where $4s^2 4p^6 5s^2$, $2s^2 2p^1$, and $2s^2 2p^2$ are treated as valence electrons for Sr, B, and C atoms, respectively. The use of the plane-wave kinetic energy cutoff of 520 eV and dense k -point sampling of $12 \times 12 \times 12$ [66], adopted here, were chosen to ensure that total energy calculations are well converged to better than 1 meV per atom. For the calculation of the density of states, we used a very dense k -point mesh of $30 \times 30 \times 30$. Electron-phonon coupling calculations for superconducting properties were performed using density-functional perturbation theory with the QUANTUM-ESPRESSO package with a k -point mesh of $4 \times 4 \times 4$ [67].

B. Experiments

High-pressure experiments were performed using BX90-style diamond-anvil cells [68] with 300- μm culets. A CuBe gasket was indented to a thickness of $\sim 40 \mu\text{m}$ and the indentation section was removed by laser drilling. The hole was backfilled with a cBN-epoxy mixture and reindented to a thickness of $\sim 40 \mu\text{m}$ to produce an electrically insulating gasket, in which a $\sim 150\text{-}\mu\text{m}$ -diameter hole was drilled for the sample chamber. The gasket was then mounted on a 3D-printed plastic ring equipped with a double-sided, copper-clad printed circuit board (PCB) circuit board, with prearranged electrical contact pads. This entire assembly was then press-fit around the diamond seat on the cell piston for reproducible placement of the gasket hole over the diamond culet, which is crucial for centering the electrical contacts on top of a sapphire thermal insulation disk. To prepare the electrical contacts, four 25- μm -thick Pt wires were cut and pressed into the cBN-epoxy gasket so that the tips were centered within the sample chamber. These contacts were then soldered to the PCB board (to which longer wires were soldered), and the whole assembly may be reproducibly placed over the diamond culets, on which $\sim 5\text{--}10\text{-}\mu\text{m}$ -thick thermally insulating sapphire crystals were placed.

The sample precursor was prepared by ball milling a mixture of SrC₂, SrB₆, and C, as described in Ref. [69]. A $\sim 100\text{-}\mu\text{m}$ -diameter precursor pellet was then loaded into the sample chamber within an inert Ar glovebox (on top of the lower sapphire crystal, and between the electrodes), and the top diamond (with top sapphire crystal) was then lowered into the gasket to seal the sample between the insulating crystals. The ruby and the diamond pressure scales were used to calibrate pressure during sample loading and unloading [70,71], and the Ne-calibrated [69] equation of state for SrB₃C₃ was used to determine pressure with *in situ* x-ray diffraction.

After compression to $\sim 50\text{--}60$ GPa, samples were measured using synchrotron x-ray diffraction with *in situ* infrared laser (1064 nm) heating at sectors 16-ID-B, HPCAT, and 13-ID-D, GSECARS, Advanced Photon Source, Argonne National Laboratory. A tightly focused flat-top infrared laser ($\sim 10\text{-}\mu\text{m}$ -diameter spot) was focused on the sample between the Pt electrodes, and the power was incremented to generate high temperatures [72]. Once temperatures near ~ 2500 K were achieved, we observed diffraction peaks that correspond to cubic SrB₃C₃, and maximal conversion was achieved at

$T > 3000$ K for ~ 20 min of continuous heating. The laser position was translated a few micrometers away from the central region between the Pt contacts to maximize conversion without heating the Pt wires. Typical samples showed ~ 60 wt. % SrB₃C₃ with unreacted SrB₆ surrounding the heated region near the contacts.

After the clathrate phase fraction was maximized by heating, the temperature was quenched to ambient and the cell was moved to an open-flow He cryostat (CryoIndustries) equipped for AC electrical transport measurements. Reported temperatures were measured using a Si diode and Lakeshore 336 controller attached to the diamond cell with Apiezon N grease, and a second diode attached to the copper cell clamp was used to monitor the temperature gradient between the cell and clamp upon heating (cooling), which was typically < 1 K. The sample contacts ($\pm I$, $\pm V$) were routed through the cryostat with an in-line 1Ω resistor to Stanford Research Systems SR830 DSP lock-in amplifier operating at 0.1–1 V in subtractive mode, and four-point resistance was measured as a function of temperature. Given the variability in resistance drop behavior due to inhomogeneities, T_c was defined as the resistance drop onset to allow for comparisons between different samples. Samples were cooled via the regulation of He gas flow ($\sim 5\text{--}20$ standard cubic feet per hour.) At temperatures below 50 K, samples were cooled at a rate of ~ 0.2 K/min to allow for thermal equilibration. Once base temperature (~ 5 K) was achieved, samples warmed naturally at a rate of ~ 0.1 K/min by removing He flow; above ~ 50 K resistive heaters were used to increase the heating rate.

Magnetic-field dependent $R(T)$ measurements were performed on a sample (Sample 3) generated within a non-magnetic CuBe cell. After verifying the presence of SrB₃C₃ between the electrical contacts via x-ray diffraction, the cell was mounted in the ³He Heliox system with 18-T magnet at the University of Maryland. Four-point AC resistance was collected during heating from base temperature (~ 4 K) in steps of ~ 0.25 K. Thermal equilibrium was established by ensuring that the heating and cooling curves were identical. Data were collected from 0–18 T in steps of 1.5 T, and in steps of 0.5 T at low field in order to define $dH_{C2}/dT|_{T=T_c}$. The resistance drop onset was used to estimate $H_{c2}(T)$ given that the base of the transition is not clearly defined beyond low field and for consistency with other data. Transition temperatures decrease by ~ 4 K when utilizing $\rho_{50\%}$ criteria for the low-field data where a transition base is defined. Differential resistivity measurements were performed as a function of temperature and magnetic field by imposing a small AC modulation on a DC voltage between contact pairs at 40 GPa.

Twelve samples were prepared in total; however, in several cases one or more of the electrical leads was severed, and no resistance drop was observed due to contact resistance effects and the incomplete conversion to the clathrate phase. The resistivity drop was only observed for samples in which all four electrodes remained intact. Attempts to make resistivity measurements on recovered samples were not successful, likely due to the reactive nature of the sample surface (samples easily hydrolyze outside of an inert environment), although x-ray-diffraction (XRD) measurements indicate the metastable persistence of SrB₃C₃ at ambient pressure under argon [59].

III. RESULTS AND DISCUSSION

We computed the electronic band structure of SrB_3C_3 clathrate using the SCAN meta-generalized gradient approximation functional [63], which was demonstrated to produce accurate electronic structures [64]. The electron deficiency of the B–C framework creates empty bands above the Fermi level. Figure 1(a) also shows the band projections onto the B $2p$ and C $2p$ orbitals. Compared to other orbitals, the $2p$ orbitals are the most dominant components of the electronic states near the Fermi level [Fig. 1(b)], indicating that the electrical transport properties are primarily controlled by the B–C framework. The band structure of SrB_3C_3 shows that the conduction behavior changes from hole-like to electron-like near the M point close to the Fermi energy, and several dispersive (steep) bands that cross the Fermi surface along R – M – Γ . These dispersive bands are responsible for conduction through the B–C framework. We note also that, as the band structure and density of states (DOS) show, one could move the Fermi level into regions of a higher DOS by electron (hole) doping from the SrB_3C_3 stoichiometry.

We next performed electron–phonon coupling calculations to investigate potential superconductivity in SrB_3C_3 [73]. Phonon dispersion relations and the phonon density of states (PHDOS) for SrB_3C_3 clathrate at 0 GPa are shown in Fig. 1(c). To illustrate the contributions associated with different phonon modes, blue circles are plotted with radii proportional to the corresponding electron–phonon coupling strength, λ . The phonon spectrum is divided into two regions by a gap at 200 cm^{-1} . The lower-frequency branch is mainly associated with phonons involving Sr atoms, while the higher-frequency branch is mainly associated with phonons involving C and B atoms. The superconducting transition temperature, T_c , was estimated from the Allen–Dynes modified McMillan equation [74]. At ambient pressure, the calculated T_c range is 27–43 K for Coulomb pseudopotential values of $\mu^* = 0.17$ – 0.10 , respectively.

According to the McMillan equation, T_c is dominated by λ , the logarithmic average of the phonon spectrum (ω_{\log}), and the DOS at the Fermi level (N_F). The electron–phonon coupling parameter λ was evaluated with the McMillan–Hopfield expression [75], from which it is clear that a large N_F has a positive contribution to λ . The calculated N_F of SrB_3C_3 is 1.2 eV^{-1} per cell at 0 GPa, which is almost completely derived from B–C bonds [Figs. 1(b) and 1(d)]. The N_F of SrB_3C_3 leads to a large λ of 0.95 compared to the value of 0.71 for MgB_2 at ambient pressure [76]. The complete mixing of B–C vibrations throughout their frequency range, except at the highest frequencies (above $\sim 700\text{ cm}^{-1}$), contributes 86% of the total magnitude of λ [Fig. 1(c)]. In contrast, the low-frequency Sr translational vibrations (below 200 cm^{-1}) were found to only contribute $\sim 14\%$ in total to λ .

In order to test predictions of superconductivity, we developed an experimental diamond-anvil cell (DAC) technique for *in situ* electrical transport measurements on samples that require extreme synthesis conditions, e.g., 50 GPa and $> 3000\text{ K}$. The refractory nature of B and C necessitates prolonged laser heating at very high temperatures, which is not needed in high-pressure hydride experiments that only require gentle pulsed heating at moderate temperatures $< 1000\text{ K}$

(e.g., LaH_{10} [13,30]), or even simple exposure to visible laser irradiation [18]. Establishing a method to produce enough sample to satisfy the electrical transport percolation threshold required to observe superconductivity ($\sim 16\text{ vol. \%}$) [77] without melting the electrical contacts proved especially challenging. One-sided laser heating with thermal insulation was ineffective to produce enough SrB_3C_3 between electrical contacts on the nonheated anvil. Our solution was to use two single crystals of sapphire (~ 5 – $10\text{ }\mu\text{m}$ thick) that rest on top of both diamond anvils and provide thermal insulation during heating from a tightly focused infrared laser. In this case, electrical leads are placed on top of one of the sapphire crystals, as shown in Fig. 2. By heating the synthesis precursor in a ~ 10 – μm -diameter spot near $\sim 3000\text{ K}$ on both sides, we were able to produce samples containing $\sim 60\text{ wt. \%}$ SrB_3C_3 clathrate located between the Pt electrical contacts. Given the requirement for *in situ* laser heating, it was not possible for the electrical probes to make significant direct contact with the clathrate phase, and thus additional contact resistance from the unreacted precursor phase is always present during transport measurements.

After verifying high-pressure, high-temperature (HPHT) synthesis of the SrB_3C_3 clathrate phase between the electrical leads using synchrotron XRD, the DAC was placed into an open-flow He cryostat equipped for AC electrical transport measurements. The electrical resistance of the samples initially increases with decreasing temperature (Fig. 3), indicating semiconducting behavior, rather than the metallic behavior expected for the clathrate. This transport behavior is attributed to incomplete precursor conversion with unreacted glassy carbon, cubic SrB_6 , and amorphous SrC_2 , which are all resistive phases and dominate transport at the electrical contacts. Though conducting at ambient pressure, compressed glassy carbon is insulating at 50 GPa [78,79]. Upon cooling SrB_3C_3 near $\sim 20\text{ K}$, the resistance drops sharply by ~ 30 – 50% , and then either increases again with the pretransition slope or continues to fall with additional cooling to the base temperature of $\sim 5\text{ K}$ (Fig. 3). This behavior is consistent with percolative transport of a mixture of superconducting and resistive phases, the precise proportion and position of which determines the series resistance at a given temperature [80–84]. The abrupt change in resistance is reversible with heating (cooling) cycles, showing no detectable hysteresis, consistent with superconductivity, but not with a structural phase transition.

The T_c onset for different runs was estimated by extrapolating the linear regions before and after the resistance drop. At the highest synthesis pressure of 64 GPa, the experimental $T_c = 14.4\text{ K}$ is in good agreement with calculations when $\mu^* \approx 0.15$, which is in the normal range [75]. Previous McMillan fits for silicon clathrate $\text{Ba}_8\text{Si}_{46}$ [85] and germanium clathrate $\text{Ba}_{24}\text{Ge}_{100}$ [86,87] gave a range of 0.10–0.31 for μ^* . Our computational predictions indicate that T_c of SrB_3C_3 increases with decreasing pressure due to an increase in N_F , ω_{\log} , and λ [Fig. 1(d)]. The experimental resistance drops measured during sample unloading follow this calculated pressure dependence of T_c with μ^* bounded between 0.13 and 0.17 [Fig. 3(b)]. We note that during the review of this paper, a report of superconductivity in SrB_3C_3 using the anisotropic

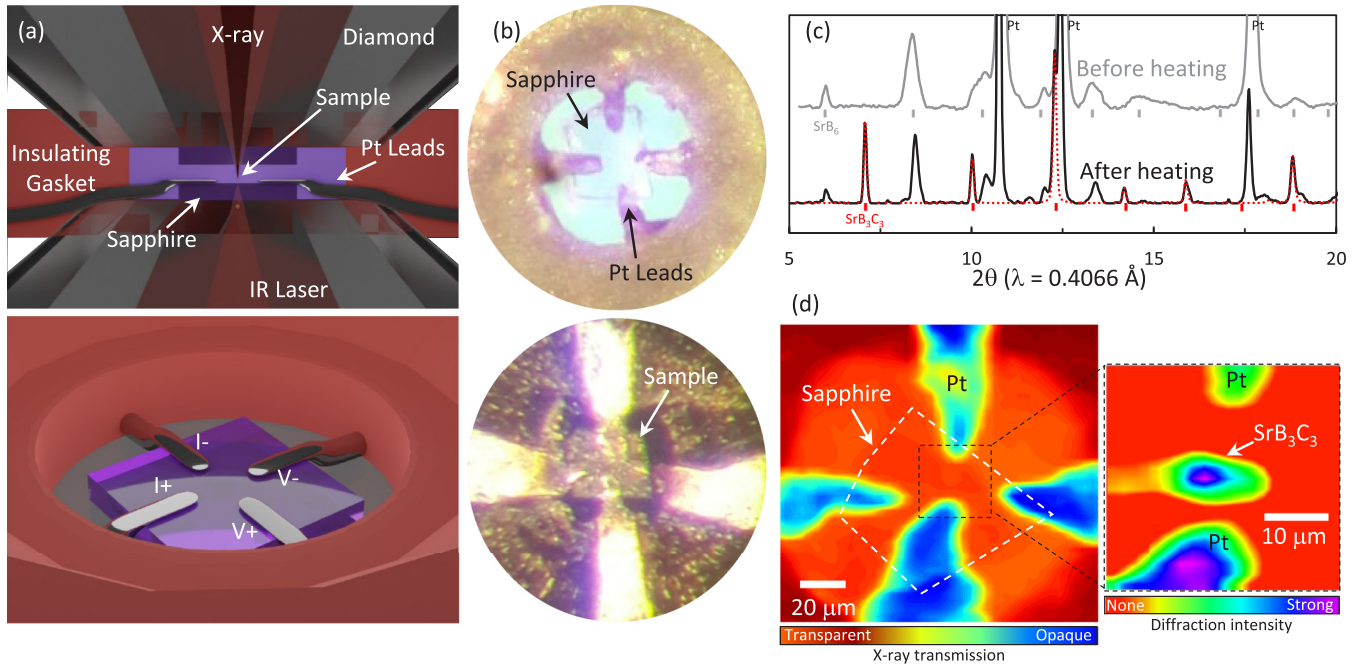


FIG. 2. (a) Sample geometry for *in situ* electrical transport with HPHT synthesis. The 1Sr:3B:3C precursor is pressed between the diamond anvils, separated by sapphire single crystals that serve as thermal insulation. Four Pt electrical probes sit on the bottom sapphire crystal and are secured within the insulating gasket. (b) Photomicrographs of the sample chamber before loading (view through top diamond), and after loading sample (view through bottom diamond). (c) Representative XRD patterns before and after heating. The heated region shows ~ 60 wt. % SrB₃C₃ with unconverted cubic SrB₆. (d) X-ray radiograph of the sample chamber with four Pt wires. Outline of the sapphire is indicated by the white dashed line. The dashed black square contains the laser-heated region between the Pt contacts. The zoom window shows an x-ray-diffraction intensity map for SrB₃C₃ and Pt showing the synthesized sample between the contacts.

Eliashberg equations [88] was published [89], which confirms our calculations with nearly identical values for T_c .

The superconducting nature of the transition was verified by repeating the electrical transport measurements under applied magnetic fields. If the transition is related to superconductivity, the transition temperature will be suppressed up to a critical field, H_{c2} , at which point superconductivity will be destroyed and the material will return to its normal conducting

state. With increasing field up to 18 T, the transition temperature is indeed suppressed by approximately -0.8 K/T , which indicates the superconducting nature of the sample (Fig. 4). The superconducting transition is further supported by differential resistance measurements, which show a peak in dV/dI at zero bias when $T < T_c$ [Figs. 4(c) and 4(d)]. This peak in the differential resistance at zero bias is attributed to strong inelastic scattering at the metal-sample interface that

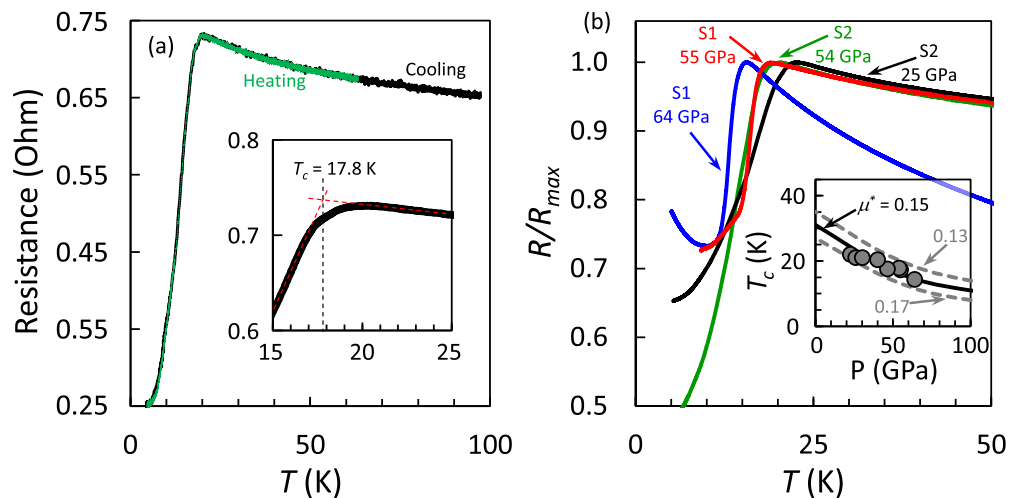


FIG. 3. (a) Resistance drop during cooling of S2 to a base temperature of 5 K at 54 GPa. The heating trace (green overlay) follows the same path with no detectable hysteresis. The inset shows the determination of the T_c onset by extrapolation of linear regions. (b) Normalized resistance for several cooling runs at different pressures for samples S1 and S2. The inset shows the pressure dependence of experimental T_c onset values for SrB₃C₃ with pressure (points) compared with calculations using different values of μ^* (lines).

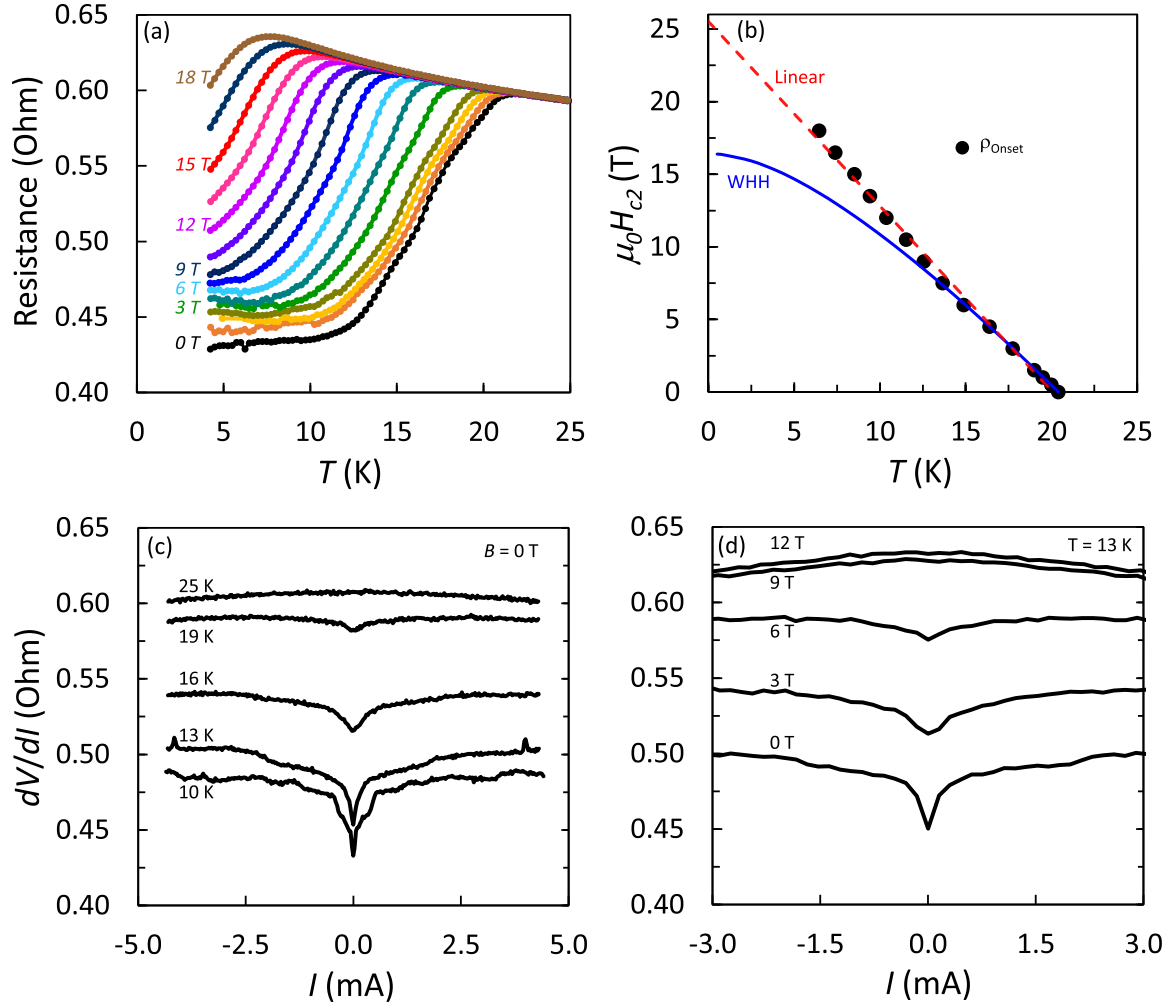


FIG. 4. (a) Resistance of sample S3 at 40 GPa as a function of temperature and magnetic field. (b) $\mu_0 H_{c2}(T)$ for the transition onset (black points) compared with the WHH model ($\alpha = 0$). A linear fit is shown to guide the eye. Differential resistance measurements performed (c) as a function of temperature at zero field and (d) as a function of field at 13 K. A peak in dV/dI appears at zero bias when $T < T_c$ and $B < \mu_0 H_{c2}$.

locally suppresses superconductivity and breaks down at the high-current limit, as often observed in the thermal limit of the Andreev reflection [90].

$H_{c2}(T)$ data determined using transition onset criteria at 40 GPa, are not described well by the Ginzberg–Landau ($1 - t^2$) model, and deviate significantly from the Werthamer–Helfand–Hohenberg (WHH) equation at fields above ~ 7 T [91,92]. This deviation, which approximates a linear trend up to 18 T, can be described by enhanced electron–phonon coupling [93] with $\lambda > 2$; however, the calculated coupling parameter of 0.95 suggests that strong coupling likely does not play a dominant role. Fermi surface anisotropy or multiband effects [94] may also serve to enhance $H_{c2}(T)$. Anisotropy was recently found to be important for SrB_3C_3 , [89] but the specific influence on $H_{c2}(T)$ is currently unknown. In addition, the granularity of the sample may also influence the behavior of the upper critical field, particularly when the grain size becomes smaller than the coherence length [95]. While similar enhancements in $H_{c2}(T)$ were observed previously for other carbon and boron-bearing superconductors [96–98] and other materials under pressure [99], additional measurements on phase-pure samples are re-

quired to further understand the origin of this behavior and whether it is intrinsic.

The agreement between experiment and calculations in both the magnitude and pressure dependence of T_c , as well as the suppression of the transition with magnetic field, provide compelling evidence that carbon-based clathrates are a promising class of superconductors. The highest T_c recorded thus far is ~ 22 K at 23 GPa. Attempts to measure the transition below ~ 20 GPa were unsuccessful due to experimental complications on decompression such as broken diamonds or loss of electrical contacts. Since XRD measurements confirm that SrB_3C_3 is recoverable to ambient pressure when held under inert conditions [59], additional measurements are needed to confirm the presence of superconductivity at 1 atm. Following the theoretical trend for $\mu^* = 0.15$, a T_c near 31 K is anticipated at ambient pressure, which is comparable to the current conventional record.

IV. SUMMARY

In summary, carbon-based clathrates represent a class of superconducting materials that can exhibit high transition

temperatures. In addition, the experimental method employed here allows for *in situ* electrical transport measurements on complex samples that require synthesis at extreme pressures near 50 GPa and extended heating at temperatures > 3000 K. The guest-host nature of the clathrate structure allows for a wide range of possible substitution schemes that can tune the electronic structure and possibly increase T_c . Recent studies suggest that hole doping with alkali metals can produce binary guest structures with transition temperatures approaching 100 K [100–102]. The possibility for such substitutions, in addition to the possibility for a large number of alternative clathrate structure types, suggests a path for light-element, covalent framework materials with high- T_c superconductivity and dynamic stability at atmospheric pressure.

ACKNOWLEDGMENTS

We thank R. Hrubiak, M. Guerette, G. M. Borstad, R. Ferry, Z. Geballe, J. Lai, and A. Karandikar for assistance with experiments; J. Rojas for assistance with graphics; and

L. Dubrovinski for providing a nonmagnetic cell. This work was supported by the U.S. Department of Energy (DOE), Office of Science, Basic Energy Sciences, under Award No. DE-SC0020683. Experiments at the University of Maryland were supported by the Gordon and Betty Moore Foundation's EPIQS Initiative through Grant No. GBMF9071. Computations were carried out at the Memex cluster of Carnegie Institution for Science. Portions of this work were performed at HPCAT (Sector 16), and GSECARS (Sector 13), Advanced Photon Source (APS), Argonne National Laboratory. HPCAT operations are supported by DOE-NNSA's Office of Experimental Sciences. GeoSoilEnviroCARS is supported by the National Science Foundation – Earth Sciences (Grant No. EAR – 1634415) and Department of Energy- GeoSciences (Grant No. DE-FG02-94ER14466). The Advanced Photon Source is a U.S. DOE Office of Science User Facility operated for the DOE Office of Science by Argonne National Laboratory under Contract No. DE-AC02-06CH11357. P.A.G. thanks Polish National Agency for Academic Exchange for financial support (PPN/BEK/2018/1/00035).

-
- [1] H. K. Onnes, Research Notebooks 56, 57, Kamerlingh Onnes Archive, Boerhaave Museum, Leiden, The Netherlands (1911).
- [2] J. G. Bednorz and K. A. Müller, Possible high T_c superconductivity in the Ba–La–Cu–O system, *Z. Phys. B: Condens Matter* **64**, 189 (1986).
- [3] G. F. Sun, K. W. Wong, B. R. Xu, Y. Xin, and D. F. Lu, T_c enhancement of HgBa₂Ca₂Cu₃O_{8+ δ} by Tl substitution, *Phys. Lett. A* **192**, 122 (1994).
- [4] Y. Kamihara, T. Watanabe, M. Hirano, and H. Hosono, Iron-based layered superconductor La[O_{1-x}Fx]FeAs ($x = 0.05$ – 0.12) with $T_c = 26$ K, *J. Am. Chem. Soc.* **130**, 3296 (2008).
- [5] Y. Kamihara, H. Hiramatsu, M. Hirano, R. Kawamura, H. Yanagi, T. Kamiya, and H. Hosono, Iron-based layered superconductor: LaOFeP, *J. Am. Chem. Soc.* **128**, 10012 (2006).
- [6] G. R. Stewart, Superconductivity in iron compounds, *Rev. Mod. Phys.* **83**, 1589 (2011).
- [7] Y. Li, G. Gao, Y. Xie, Y. Ma, T. Cui, and G. Zou, Superconductivity at ~ 100 K in dense SiH₄(H₂)₂ predicted by first principles, *Proc. Natl. Acad. Sci.* **107**, 15708 (2010).
- [8] Y. Li, J. Hao, H. Liu, Y. Li, and Y. Ma, The metallization and superconductivity of dense hydrogen sulfide, *J. Chem. Phys.* **140**, 174712 (2014).
- [9] H. Wang, J. S. Tse, K. Tanaka, T. Iitaka, and Y. Ma, Superconductive sodalite-like clathrate calcium hydride at high pressures, *Proc. Natl. Acad. Sci.* **109**, 6463 (2012).
- [10] J. A. Flores-Livas, L. Boeri, A. Sanna, G. Profeta, R. Arita, and M. Eremets, A perspective on conventional high-temperature superconductors at high pressure: Methods and materials, *Phys. Rep.* **856**, 1 (2020).
- [11] H. Liu, I. I. Naumov, R. Hoffmann, N. W. Ashcroft, and R. J. Hemley, Potential high- T_c superconducting lanthanum and yttrium hydrides at high pressure, *Proc. Natl. Acad. Sci.* **114**, 6990 (2017).
- [12] Y. Sun, J. Lv, Y. Xie, H. Liu, and Y. Ma, Route to a Superconducting Phase above Room Temperature in Electron-Doped Hydride Compounds under High Pressure, *Phys. Rev. Lett.* **123**, 097001 (2019).
- [13] M. Somayazulu, M. Ahart, A. K. Mishra, Z. M. Geballe, M. Baldini, Y. Meng, V. V. Struzhkin, and R. J. Hemley, Evidence for Superconductivity above 260 K in Lanthanum Superhydride at Megabar Pressures, *Phys. Rev. Lett.* **122**, 027001 (2019).
- [14] D. Duan, X. Huang, F. Tian, D. Li, H. Yu., Y. Liu, Y. Ma, B. Liu, and T. Cui, Pressure-induced decomposition of solid hydrogen sulfide, *Phys. Rev. B* **91**, 180502(R) (2015).
- [15] C. J. Pickard, I. Errea, and M. I. Eremets, Superconducting hydrides under pressure, *Annu. Rev. Condens. Matter Phys.* **11**, 57 (2020).
- [16] F. Peng, Y. Sun, C. J. Pickard, R. J. Needs, Q. Wu, and Y. Ma, Hydrogen Clathrate Structures in Rare Earth Hydrides at High Pressures: Possible Route to Room-Temperature Superconductivity, *Phys. Rev. Lett.* **119**, 107001 (2017).
- [17] H. Xie *et al.*, Hydrogen Pentagraphenelike Structure Stabilized by Hafnium: A High-Temperature Conventional Superconductor, *Phys. Rev. Lett.* **125**, 217001 (2020).
- [18] E. Snider, N. Dasenbrock-Gammon, R. McBride, M. Debessai, H. Vindana, K. Vencatasamy, K. V. Lawler, A. Salamat, and R. P. Dias, Room-temperature superconductivity in a carbonaceous sulfur hydride, *Nature (London)* **586**, 373 (2020).
- [19] Y. Sun, Y. Tian, B. Jiang, X. Li, H. Li, T. Iitaka, X. Zhong, and Y. Xie, Computational discovery of a dynamically stable cubic SH₃-like high-temperature superconductor at 100 GPa via CH₄ intercalation, *Phys. Rev. B* **101**, 174102 (2020).
- [20] W. Cui, T. Bi, J. Shi, Y. Li, H. Liu, E. Zurek, and R. J. Hemley, Route to high- T_c superconductivity via CH₄-Intercalated H₃S hydride perovskites, *Phys. Rev. B* **101**, 134504 (2020).
- [21] J. Bardeen, L. N. Cooper, and J. R. Schrieffer, Theory of superconductivity, *Phys. Rev.* **108**, 1175 (1957).

- [22] G. Eliashberg, Interactions between electrons and lattice vibrations in a superconductor, *J. Exp. Theor. Phys.* **38**, 966 (1960).
- [23] W. E. Pickett, Colloquium: Room temperature superconductivity: The roles of theory and materials design, *Rev. Mod. Phys.* (2022).
- [24] N. W. Ashcroft, Metallic Hydrogen: A High-Temperature Superconductor? *Phys. Rev. Lett.* **21**, 1748 (1968).
- [25] N. W. Ashcroft, Hydrogen Dominant Metallic Alloys: High Temperature Superconductors? *Phys. Rev. Lett.* **92**, 187002 (2004).
- [26] D. Duan, Y. Liu, F. Tian, D. Li, X. Huang, Z. Zhao, H. Yu, B. Liu, W. Tian, and T. Cui, Pressure-induced metallization of dense $(\text{H}_2\text{S})_2\text{H}_2$ with high- T_c superconductivity, *Sci. Rep.-UK* **4**, 6968 (2014).
- [27] I. Troyan, A. Gavriluk, R. Ruffer, A. Chumakov, A. Mironovich, I. Lyubutin, D. Perekalin, A. P. Drozdov, and M. I. Eremets, Observation of superconductivity in hydrogen sulfide from nuclear resonant scattering, *Science* **351**, 1303 (2016).
- [28] A. P. Drozdov, M. I. Eremets, I. A. Troyan, V. Ksenofontov, and S. I. Shylin, Conventional superconductivity at 203 kelvin at high pressures in the sulfur hydride system, *Nature (London)* **525**, 73 (2015).
- [29] I. Errea *et al.*, Quantum crystal structure in the 250-kelvin superconducting lanthanum hydride, *Nature (London)* **578**, 66 (2020).
- [30] A. P. Drozdov *et al.*, Superconductivity at 250 k in lanthanum hydride under high pressures, *Nature (London)* **569**, 528 (2019).
- [31] C. J. Pickard and R. J. Needs, High-Pressure Phases of Silane, *Phys. Rev. Lett.* **97**, 045504 (2006).
- [32] M. I. Eremets, I. A. Trojan, S. A. Medvedev, J. S. Tse, and Y. Yao, Superconductivity in hydrogen dominant materials: Silane, *Science* **319**, 1506 (2008).
- [33] G. Gao, A. R. Oganov, A. Bergara, M. Martinez-Canales, T. Cui, T. Iitaka, Y. Ma, and G. Zou, Superconducting High Pressure Phase of Germane, *Phys. Rev. Lett.* **101**, 107002 (2008).
- [34] G. Gao *et al.*, High-pressure crystal structures and superconductivity of stannane (SnH_4), *Proc. Natl. Acad. Sci.* **107**, 1317 (2010).
- [35] B. Chen, L. J. Conway, W. Sun, X. Kuang, C. Lu, and A. Hermann, Phase stability and superconductivity of lead hydrides at high pressure, *Phys. Rev. B* **103**, 035131 (2021).
- [36] P. Zaleski-Ejgierd, R. Hoffmann, and N. W. Ashcroft, High Pressure Stabilization and Emergent Forms of PbH_4 , *Phys. Rev. Lett.* **107**, 037002 (2011).
- [37] M. Beekman and G. S. Nolas, Inorganic clathrate-II materials of group 14: Synthetic routes and physical properties, *J. Mater. Chem.* **18**, 842 (2007).
- [38] G. S. Nolas, J. L. Cohn, G. A. Slack, and S. B. Schujman, Semiconducting Ge clathrates: Promising candidates for thermoelectric applications, *Appl. Phys. Lett.* **73**, 178 (1998).
- [39] J. S. Kasper, P. Hagenmuller, M. Pouchard, and C. Cros, Clathrate structure of silicon $\text{Na}_8\text{Si}_{46}$ and $\text{Na}_x\text{Si}_{136}$ ($x < 11$), *Science* **150**, 1713 (1965).
- [40] R. Kröner, K. Peters, H. G. von Schnering, and R. Nesper, Crystal structure of the clathrate-II, $\text{Ba}_{16}\text{Ga}_{32}\text{Sn}_{104}$, *Z. Kristall. - New Cryst. Struct.* **213**, 704 (1998).
- [41] A. M. Guloy, R. Ramlau, Z. Tang, W. Schnelle, M. Baitinger, and Y. Grin, A guest-free germanium clathrate, *Nature (London)* **443**, 320 (2006).
- [42] A. J. Karttunen, T. F. Fässler, M. Linnolahti, and T. A. Pakkanen, Structural principles of semiconducting group 14 clathrate frameworks, *Inorg. Chem.* **50**, 1733 (2011).
- [43] J. Nagamatsu, N. Nakagawa, T. Muranaka, Y. Zenitani, and J. Akimitsu, Superconductivity at 39 K in magnesium diboride, *Nature (London)* **410**, 63 (2001).
- [44] T. Sakai, G.-Y. Adachi, and J. Shiokawa, Electrical properties of rare earth diborodiborides (RB_2C_2 -type layer compounds), *J. Less Common Metals* **84**, 107 (1982).
- [45] A. K. Verma, P. Modak, D. M. Gaitonde, R. S. Rao, B. K. Godwal, and L. C. Gupta, Possible high-temperature superconductivity in hole-doped, *Europhys. Lett.* **63**, 743 (2003).
- [46] E. Spanò, M. Bernasconi, and E. Kopnin, Electron-phonon interaction in hole-doped MgB_2C_2 , *Phys. Rev. B* **72**, 014530 (2005).
- [47] Q. Li, H. Wang, Y. Tian, Y. Xia, T. Cui, J. He, Y. Ma, and G. Zou, Superhard and superconducting structures of BC_5 , *J. Appl. Phys.* **108**, 023507 (2010).
- [48] Y. Yao, J. S. Tse, and D. D. Klug, Crystal and electronic structure of superhard BC_5 : First-principles structural optimizations, *Phys. Rev. B* **80**, 094106 (2009).
- [49] H. Liu, Q. Li, L. Zhu, and Y. Ma, Superhard and superconductive polymorphs of diamond-like BC_3 , *Phys. Lett. A* **375**, 771 (2011).
- [50] M. Kosaka, K. Tanigaki, K. Prassides, S. Margadonna, A. Lappas, C. M. Brown, and A. N. Fitch, Superconductivity in $\text{Li}_x\text{CsC}_{60}$ Fullerides, *Phys. Rev. B* **59**, R6628(R) (1999).
- [51] C. Liu, X. Song, Q. Li, Y. Ma, and C. Chen, Superconductivity in Compression-Shear Deformed Diamond, *Phys. Rev. Lett.* **124**, 147001 (2020).
- [52] S. Saha, S. Di Cataldo, M. Amsler, W. v. d. Linden, and L. Boeri, High-temperature conventional superconductivity in the boron-carbon system: Material trends, *Phys. Rev. B* **102**, 024519 (2020).
- [53] S. Lu, H. Liu, I. I. Naumov, S. Meng, Y. Li, J. S. Tse, B. Yang, and R. J. Hemley, Superconductivity in dense carbon-based materials, *Phys. Rev. B* **93**, 104509 (2016).
- [54] F. Zipoli, M. Bernasconi, and G. Benedek, Electron-phonon coupling in halogen-doped carbon clathrates from first principles, *Phys. Rev. B* **74**, 205408 (2006).
- [55] X. Blase, E. Bustarret, C. Chapelier, T. Klein, and C. Marcatat, Superconducting group-IV semiconductors, *Nat. Mater.* **8**, 375 (2009).
- [56] Y. Wang, J. Lv, L. Zhu, and Y. Ma, Crystal structure prediction via particle-swarm optimization, *Phys. Rev. B* **82**, 094116 (2010).
- [57] Y. Wang, J. Lv, L. Zhu, and Y. Ma, CALYPSO: A method for crystal structure prediction, *Comput. Phys. Commun.* **183**, 2063 (2012).
- [58] B. Gao, P. Gao, S. Lu, J. Lv, Y. Wang, and Y. Ma, Interface structure prediction via CALYPSO method, *Sci. Bull.* **64**, 301 (2019).
- [59] L. Zhu *et al.*, Carbon-boron clathrates as a new class of sp^3 -Bonded framework materials, *Sci. Adv.* **6**, eaay8361 (2020).
- [60] J. P. Perdew, K. Burke, and M. Ernzerhof, Generalized Gradient Approximation Made Simple, *Phys. Rev. Lett.* **77**, 3865 (1996).

- [61] J. P. Perdew and Y. Wang, Accurate and simple analytic representation of the electron-gas correlation energy, *Phys. Rev. B* **45**, 13244 (1992).
- [62] G. Kresse and J. Furthmüller, Efficient iterative schemes for ab initio total-energy calculations using a plane-wave basis set, *Phys. Rev. B* **54**, 11169 (1996).
- [63] J. Sun, A. Ruzsinszky, and J. P. Perdew, Strongly Constrained and Appropriately Normed Semilocal Density Functional, *Phys. Rev. Lett.* **115**, 036402 (2015).
- [64] J. Sun *et al.*, Accurate first-principles structures and energies of diversely bonded systems from an efficient density functional, *Nat. Chem.* **8**, 831 (2016).
- [65] P. E. Blöchl, Projector augmented-wave method, *Phys. Rev. B* **50**, 17953 (1994).
- [66] H. J. Monkhorst and J. D. Pack, Special points for Brillouin-zone integrations, *Phys. Rev. B* **13**, 5188 (1976).
- [67] P. Giannozzi *et al.*, QUANTUM ESPRESSO: A modular and open-source software project for quantum simulations of materials, *J. Phys.: Condens. Matter* **21**, 395502 (2009).
- [68] I. Kantor, V. Prakapenka, A. Kantor, P. Dera, A. Kurnosov, S. Sinogeikin, N. Dubrovinskaya, and L. Dubrovinsky, BX90: A new diamond anvil cell design for x-ray diffraction and optical measurements, *Rev. Sci. Instrum.* **83**, 125102 (2012).
- [69] A. Dewaele, F. Datchi, P. Loubeyre, and M. Mezouar, High pressure–high temperature equations of state of neon and diamond, *Phys. Rev. B* **77**, 094106 (2008).
- [70] H. K. Mao, J. Xu, and P. M. Bell, Calibration of the ruby pressure gauge to 800 kbar under quasi-hydrostatic conditions, *J. Geophys. Res. Solid Earth* **91**, 4673 (1986).
- [71] Y. Akahama and H. Kawamura, Pressure calibration of diamond anvil Raman gauge to 310 GPa, *J. Appl. Phys.* **100**, 043516 (2006).
- [72] Y. Meng, R. Hrubiak, E. Rod, R. Boehler, and G. Shen, New developments in laser-heated diamond anvil cell with in situ synchrotron x-ray diffraction at high pressure collaborative access team, *Rev. Sci. Instrum.* **86**, 072201 (2015).
- [73] L. Zhu, H. Liu, R. E. Cohen, R. Hoffmann, and T. A. Strobel, Prediction of a thermodynamically stable carbon-based clathrate, [arXiv:1708.03483v1](https://arxiv.org/abs/1708.03483v1) (2017).
- [74] P. B. Allen and R. C. Dynes, Transition temperature of strong-coupled superconductors reanalyzed, *Phys. Rev. B* **12**, 905 (1975).
- [75] W. L. McMillan, Transition temperature of strong-coupled superconductors, *Phys. Rev.* **167**, 331 (1968).
- [76] Y. Wang, J. Lv, Y. Ma, T. Cui, and G. Zou, Superconductivity of MgB₂ under ultrahigh pressure: A first-principles study, *Phys. Rev. B* **80**, 092505 (2009).
- [77] A. L. Efros and B. I. Shklovskii, Critical behaviour of conductivity and dielectric constant near the metal-non-metal transition threshold, *Phys. Status Solidi B* **76**, 475 (1976).
- [78] Y. Lin, L. Zhang, H.-k. Mao, P. Chow, Y. Xiao, M. Baldini, J. Shu, and W. L. Mao, Amorphous Diamond: A High-Pressure Superhard Carbon Allotrope, *Phys. Rev. Lett.* **107**, 175504 (2011).
- [79] M. Yao, J. Xiao, X. Fan, R. Liu, and B. Liu, Transparent, superhard amorphous carbon phase from compressing glassy carbon, *Appl. Phys. Lett.* **104**, 021916 (2014).
- [80] K. N. R. Taylor, D. S. Misra, D. N. Matthews, and G. Alvarez, The percolation limit and weak link effects on the superconducting phase transition in high temperature superconductors, *Phase Transit.* **22**, 103 (1990).
- [81] M. J. R. Sandim, P. A. Suzuki, S. Spagna, S. C. Tripp, R. E. Sager, and R. F. Jardim, Increased resistance below the superconducting transition in granular Sm_{1.83}Ce_{0.17}CuO_{4-y} compounds, *Phys. C Supercond.* **289**, 265 (1997).
- [82] T. H. Lin, X. Y. Shao, M. K. Wu, P. H. Hor, X. C. Jin, C. W. Chu, N. Evans, and R. Bayuzick, Observation of a reentrant superconducting resistive transition in granular BaPb_{0.75}Bi_{0.25}O₃ superconductor, *Phys. Rev. B* **29**, 1493(R) (1984).
- [83] H. M. Seyoum, A. M. Riitano, L. H. Bennett, and W. Wong-Ng, Evidence suggesting reentrant superconductivity in a multiphase Tl-Ca-Ba-Cu-O system, *Phys. Lett. A* **190**, 483 (1994).
- [84] G. F. Dionne, Resistivity of multiphase high-T_c superconductors, *J. Appl. Phys.* **69**, 4883 (1991).
- [85] K. Tanigaki, T. Shimizu, K. M. Itoh, J. Teraoka, Y. Moritomo, and S. Yamanaka, Mechanism of superconductivity in the polyhedral-network compound Ba₃Si₄₆, *Nat. Mater.* **2**, 653 (2003).
- [86] H. Q. Yuan, F. M. Grosche, W. Carrillo-Cabrera, V. Pacheco, G. Sparrn, M. Baenitz, U. Schwarz, Yu. Grin, and F. Steglich, Interplay of superconductivity and structural phase transition in the clathrate Ba₆Ge₂₅, *Phys. Rev. B* **70**, 174512 (2004).
- [87] R. Viennois, P. Toulemonde, C. Paulsen, and A. San-Miguel, Superconductivity in the Ba₂₄Si₁₀₀ cubic clathrate with sp² and sp³ silicon bondings, *J. Phys.: Condens. Matter* **17**, L311 (2005).
- [88] H. J. Choi, M. L. Cohen, and S. G. Louie, Anisotropic Eliashberg theory of MgB₂: T_c, isotope effects, superconducting energy gaps, quasiparticles, and specific heat, *Phys. C Supercond.* **385**, 66 (2003).
- [89] J.-N. Wang, X.-W. Yan, and M. Gao, High-Temperature superconductivity in SrB₃C₃ and BaB₃C₃ predicted from first-principles anisotropic Migdal-Eliashberg theory, *Phys. Rev. B* **103**, 144515 (2021).
- [90] L. Aggarwal, A. Gaurav, G. S. Thakur, Z. Haque, A. K. Ganguli, and G. Sheet, Unconventional superconductivity at mesoscopic point contacts on the 3D Dirac semimetal Cd₃As₂, *Nat. Mater.* **15**, 32 (2016).
- [91] E. Helfand and N. R. Werthamer, Temperature and purity dependence of the superconducting critical field, H_{c2}. II, *Phys. Rev.* **147**, 288 (1966).
- [92] N. R. Werthamer, E. Helfand, and P. C. Hohenberg, Temperature and purity dependence of the superconducting critical field, H_{c2}. III. electron spin and spin-orbit effects, *Phys. Rev.* **147**, 295 (1966).
- [93] L. N. Bulaevskii, O. V. Dolgov, and M. O. Ptitsyn, Properties of strong-coupled superconductors, *Phys. Rev. B* **38**, 11290 (1988).
- [94] L. Kuerten, E. Fillis-Tsirakis, C. Richter, J. Mannhart, and H. Boschker, Linear temperature dependence of the upper critical field across the dome of the LaAlO₃-SrTiO₃ interface superconductor, *Phys. Rev. B* **98**, 054509 (2018).
- [95] P. G. de Gennes and M. Tinkham, Magnetic behavior of very small superconducting particles, *Phys. Phys. Fiz.* **1**, 107 (1964).
- [96] G. S. Boebinger, T. T. M. Palstra, A. Passner, M. J. Rosseinsky, D. W. Murphy, and I. I. Mazin, Evidence of

- upper-critical-field enhancement in K_3C_{60} powders, *Phys. Rev. B* **46**, 5876 (1992).
- [97] J. S. Kim *et al.*, Strong electron-phonon coupling in the rare-earth carbide superconductor La_2C_3 , *Phys. Rev. B* **76**, 014516 (2007).
- [98] A. A. Castro, O. Olicón, R. Escamilla, and F. Morales, Critical temperature and upper critical field of $Li_2Pd_{3-x}Cu_xB$ ($x = 0.0, 0.1, 0.2$) superconductors, *Solid State Commun.* **255-256**, 11 (2017).
- [99] K. Kirshenbaum, P. S. Syers, A. P. Hope, N. P. Butch, J. R. Jeffries, S. T. Weir, J. J. Hamlin, M. B. Maple, Y. K. Vohra, and J. Paglione, Pressure-Induced Unconventional Superconducting Phase in the Topological Insulator Bi_2Se_3 , *Phys. Rev. Lett.* **111**, 087001 (2013).
- [100] P. Zhang, X. Li, X. Yang, H. Wang, Y. Yao, and H. Liu, Path to high- T_c superconductivity via Rb substitution of guest metal atoms in the SrB_3C_3 clathrate, *Phys. Rev. B* **105**, 094503 (2022).
- [101] S. Di Cataldo, S. Qulaghasi, G. B. Bachelet, and L. Boeri, High- T_c superconductivity in doped boron-carbon clathrates, *Phys. Rev. B* **105**, 064516 (2022).
- [102] N. Geng, K. P. Hilleke, L. Zhu, X. Wang, T. A. Strobel, and E. Zurek, Conventional High-Temperature Superconductivity in Metallic, Covalently Bonded, Binary-Guest C-B Clathrates, *J. Am. Chem. Soc.* (2023), doi: [10.1021/jacs.2c10089](https://doi.org/10.1021/jacs.2c10089)